Cell Calcium 54 (2013) 175–185

Contents lists available at ScienceDirect

Cell Calcium

journal homepage: www.elsevier.com/locate/ceca

A novel homology model of TRPC3 reveals allosteric coupling between gate and selectivity filter

Michaela Lichtenegger[a], Thomas Stockner[b], Michael Poteser[d], Hannes Schleifer[d], Dieter Platzer[d], Christoph Romanin[c], Klaus Groschner[d,*]

[a] Institute of Pharmaceutical Sciences – Pharmacology and Toxicology, University of Graz, A-8010 Graz, Austria
[b] Institute of Pharmacology, Center for Physiology and Pharmacology, Medical University of Vienna, A-1090 Wien, Austria
[c] Institute of Biophysics, University of Linz, A-4040 Linz, Austria
[d] Institute of Biophysics, Medical University of Graz, A-8010 Graz, Austria

ARTICLE INFO

Article history:
Received 15 May 2013
Received in revised form 27 May 2013
Accepted 30 May 2013
Available online 22 June 2013

Keywords:
TRPC3
Homology modeling
Selectivity
Gating

ABSTRACT

Utilizing a novel molecular model of TRPC3, based on the voltage-gated sodium channel from *Arcobacter butzleri* (Na_VAB) as template, we performed structure-guided mutagenesis experiments to identify amino acid residues involved in divalent permeation and gating. Substituted cysteine accessibility screening within the predicted selectivity filter uncovered amino acids 629–631 as the narrowest part of the permeation pathway with an estimated pore diameter of <5.8 Å. E630 was found to govern not only divalent permeability but also sensitivity of the channel to block by ruthenium red. Mutations in a hydrophobic cluster at the cytosolic termini of transmembrane segment 6, corresponding to the S6 bundle crossing structure in Na_VAB, distorted channel gating. Removal of a large hydrophobic residue (I667A or I667E) generated channels with approximately 60% constitutive activity, suggesting I667 as part of the dynamic structure occluding the permeation path. Destabilization of the gate was associated with reduced Ca^{2+} permeability, altered cysteine cross-linking in the selectivity filter and promoted channel block by ruthenium red. Collectively, we present a structural model of the TRPC3 permeation pathway and localize the channel's selectivity filter and the occluding gate. Moreover, we provide evidence for allosteric coupling between the gate and the selectivity filter in TRPC3.

1. Introduction

TRPC proteins contribute to spatial control of cytoplasmic Ca^{2+}- and Na^+-gradients as well as membrane potential by formation of non-selective cation channels that are functionally coupled to other plasma membrane ion transport systems [1–3]. Thereby, these channels control global as well as local Ca^{2+}-homeostasis of excitable and non-excitable cells in a rather complex manner. The capability to introduce simultaneous Ca^{2+}- and Na^+-entry into cells has been recognized as a potentially important mechanism for signal diversification [4]. Our understanding of the molecular basis of this feature and our picture of the architecture of the permeation pathway in TRPC channels is still incomplete. So far, structural information from crystallography is lacking and only a few functional domains have been identified, based on homology modeling and site-directed mutagenesis [5–8]. A conserved LFW motif was previously discovered as a potential key element of the permeation pathway. Mutations in the LFW motif completely disrupt channel function in a dominant negative manner, conferring permeation deficiency also to heteromers with wild type proteins [5,6]. This feature is consistent with a central position of the LFW sequence within the channel's pore complex. Nonetheless, a role of the LFW motif in specific channel functions such as selectivity or gating has not been demonstrated. Analyzing the putative pore domain in TRPC channels by mutational neutralization of charged residues identified structural features essential for Ca^{2+}-permeation. For TRPC1, negative charges close to the putative pore helix have been found to determine cation selectivity [6]. Neutralization of these charges causes a clear reduction of the TRPC1-dependent Ca^{2+}-permeability measured in human salivary glands upon heterologous expression of the mutants. Similarly, mutational analysis has uncovered a glutamate residue, that is conserved within the

Abbreviations: BAPTA, 1,2-bis(o-aminophenoxy)ethane-N,N,N′,N′-tetraacetic acid; GPCR, G protein coupled receptor; PLC, phospholipase C; DAG, diacylglycerol; SAG, 1-stearoyl-2-arachidonoyl-sn-glycerol.

* Corresponding author at: Institute of Biophysics, Medical University of Graz, Harrachgasse 21/IV, 8010 Graz, Austria. Tel.: +43 316 380 4137; fax: +43 316 380 9660.
E-mail address: klaus.groschner@medunigraz.at (K. Groschner).

0143-4160
http://dx.doi.org/10.1016/j.ceca.2013.05.010

pore domain of TRPC3/6/7 and *Drosophila* TRP, as a critical element in the selectivity filter in the *Drosophila* TRP [8]. Based on molecular modeling using KcsA and $K_V1.2$ as template structures, this acidic residue within the central part of the permeation pathway has been identified as key determinant of divalent permeation in TRPC3 [7]. Unfortunately, TRPC molecular models using KcsA or $K_V1.2$ as template suffer essentially from insufficient homology and lack definition. It appears important to consider that permeability properties may be affected by amino acid exchanges in domains distant to but structurally associated with the selectivity filter. Specifically, gating properties may impact on ion selectivity as recently documented for the Orai1 channel [9]. To obtain a more complete picture of the permeation pathway in TRPC3, we set out to explore structural elements in the pore domain by a structure-guided mutagenesis approach, adopting recently published structural information of the bacterial voltage-gated sodium channel Na_VAB [10] for molecular modeling. Our functional analysis of TRPC3 pore mutants clearly demonstrates suitability of the Na_VAB template and confirms E630 as a key residue in the channel's selectivity filter. Furthermore we identify a region forming the occluding gate and suggest a close structural relation and functional coupling between TRPC3 gate and selectivity filter.

2. Methods

2.1. Molecular biology

Site directed mutagenesis was performed using the QuickChange II Site Directed Mutagenesis Kit (Stratagene) according to the manufacturers instructions. Mutagenic primer pairs were designed by the QuickChange Primer Design Program® and synthesized by genXpress® (VWR). Human TRPC3 (UniProtKB ID: Q13507-3) cloned into pEYFP-C1 vector served as a template, resulting in a fusion protein N-terminally tagged to YFP. All mutations were confirmed by sequencing the corresponding cDNAs.

2.2. Cell culture and transfection

Human embryonic kidney 293 (HEK293) cells were cultured at 37 °C and 5% CO_2 in Dulbeco's Modified Eagle Medium (DMEM high glucose with pyruvate, Invitrogen) supplemented with streptomycin (100 μg/ml), penicillin (100 U/ml), L-glutamine (2 mM), HEPES (10 mM) and 10% fetal calf serum. Cells were transiently transfected using FuGENE® HD Transfection Reagent (Promega) as recommended by the vendor. In brief, 200 μl Opti-MEM® (Invitrogen) and 5 μg DNA was mixed thoroughly and then 6 μl transfection reagent was added. After mixing, samples were incubated for 15 min at room temperature and subsequently added to cells grown in 35 mm-dishes. Cells were harvested and plated to cover slips 24 h after transfection and finally subjected to whole-cell patch clamp experiments 48 h after transfection.

2.3. Homology modeling

Phylogenetic analysis [11] revealed that TRP channels are evolutionary related to the calcium and the sodium channels, diverging early in evolution from the very diverse class of potassium channels. We selected the Na_VAB channel as template because evolutionary this is the most related channel crystallized so far. Sequence alignment between Na_VAB and TRPC channels was carried out using muscle 3.7 [12]. The asparagine residue in helix S6, conserved in all calcium and the sodium channels allowed for an unambiguous alignment of the innermost transmembrane helix. Hydrophathy analysis, biophysical properties of membrane exposure and protein interior orientation were as much taken into account as helix capping or termination signals [13] for a manual adjustment of the full sequence alignment, necessary because of the low sequence homology between Na_VAB and TRPC channels. The model of the human TRPC3 ion channel (UniProtKB ID: Q13507-3) was based on the Na_VAB crystal structure (PDB ID: 3RVY) [10] with a resolution of 2.7 Å. Modeling was carried out with MODELLER (version 9v8) [14] applying the automodel protocol. Fifty models were generated. Model quality was assessed using the DOPE score [15] and ProCheck [16]. The best TRPC3 model had a DOPE score of −35341 (Na_VAB template's DOPE score is −41631). The Ramachandran plot of TPRC3 showed 90.9% of residues in the most favorable region, 5.6% in the allowed region, 1.4% in the generously allowed region and 2.0% in the disallowed region, while the Na_VAB template had values of 89.1%, 9.4%, 0.5% and 1.0%, respectively. The model with the best DOPE score was selected for visualization and analysis.

2.4. Electrophysiology

Patch pipettes were pulled from thin-wall filament glass capillaries GC 150TF-7.5 (Havard Apparatus) to a resistance of 3–4 MΩ. A Diaphot Inverted Tissue Culture Microscope (Nikon) was used to identify positively transfected cells by their green fluorescence when illuminated at 514 nm. Whole-cell voltage-clamp experiments were performed at room temperature using a L/A-EPC7-Amplifier (List Medical Electronic) connected with a Digidata-1322A Digitizer (Axon Instruments). Currents were filtered at 3 kHz by a 3-pole Bessel filter and digitized with 8 kHz. Application of linear voltage-ramp protocols ranging from −130 to +80 mV (holding potential 0 mV) was controlled by Clampex 9.2 (Axon Instruments) software.

2.5. Solutions and materials

The standard extracellular solution contained (in mM): 140 NaCl, 10 Hepes, 10 Glucose, 2 Mg_2Cl, 2 Ca_2Cl titrated to pH 7.4 with NMDG. In order to determine permeability of organic cations, experiments were carried out in standard extracellular solution with sodium (Na^+, diameter $d = 1.90$ Å) equimolarly replaced by di- (DMA^+, $d = 4.6$ Å), tri- ($TriMA^+$, $d = 5.2$ Å) or tetra-methyl ammonium ($TetMA^+$, $d = 5.8$ Å) [17]. In order to ensure integrity of channel function, solutions furthermore exhibited physiological concentrations of Ca^{2+} and Mg^{2+} (2 mM each). For measuring currents carried by various monovalent cations, NaCl was equimolarly replaced by LiCl, KCl, CsCl, RbCl or NMDG. The standard intracellular solution contained (in mM): 120 cesium methanesulfonate, 20 CsCl, 15 HEPES, 5 $MgCl_2$, 3 EGTA titrated to pH 7.3 with CsOH. For Ca^{2+}-permeability measurements, solutions were modified as follows: 140 mM NMDG and 10 mM Ca^{2+} extracellularly, 10 mM BAPTA intracellularly and 10 mM Cl^- symmetrically in order to eliminate chloride currents. ECS was pH-adjusted to 7.4 with methanesulfonic acid. Standard chemicals used for solutions as well as carbachol and dithiothreitol were purchased from Sigma Aldrich. Ruthenium red was purchased from Tocris Bioscience.

2.6. Epifluorescence and TIRF microscopy

Fluorescence microscopy was performed using a Zeiss Axiovert Observer D microscope, equipped with a 488 nm and 445 nm laser excitation device and a Hamamatsu Orca D2 camera system. The system is equipped with a 100× objective and condenser/beam deflector (Visitron Systems) for total internal reflection (TIRF) microscopy.

2.7. Data analysis and statistics

Data analysis and graphical display was done using Clampfit 9.2 (Axon Instruments), OriginPro8 (OriginLab Corporation) and

PyMOL (DeLano Scientific LLC, Schrödinger) software. Data are expressed as mean ± S.E.M. Student's two-sample *t*-test was used to assess statistical significance ($^{*}p < 0.05$, $^{**}p < 0.01$, $^{***}p < 0.001$.).

3. Results

3.1. E630 and V631 form the narrowest region of the open TRPC3 pore

To identify amino acids and structural motifs relevant for selectivity and gating in the TRPC3 cation channel, we first generated a molecular model of the TRPC3 pore region using a novel alignment strategy [18] and the recently crystallized voltage-gated sodium channel Na_VAB as template architecture. Fig. 1 shows our computational pore model and a sequence alignment (Fig. 1B) of mammalian TRPC isoforms along with KcsA, $K_V1.2$ and our template molecule Na_VAB. TRPC3 has been characterized as a non-selective cation channel displaying moderate preference for calcium over monovalent cations with a permeability ratio of PCa/PNa = 1.62 [19]. Discrimination between different cation species is governed by a selectivity filter, which according to our homology TRPC3 model (Fig. 1C) was suggested as a non-helical stretch of 13 amino acids (629–641) within the putative pore loop (p-loop) connecting transmembrane segments 5 and 6 (TM5–TM6) as depicted in Fig. 1C. Recent mutagenesis studies identified a glutamate residue (E630) within this stretch as an essential element of the channel's selectivity filter. Neutralization of this negative charge abolished Ca^{2+}-permeation through the channel [7]. Inherent to the concept of a selectivity filter, the hypothetical p-loop is expected to form the narrowest part of the permeation pathway in the open conformation. In an attempt to test this prediction, we performed further structure-guided mutagenesis in terms of an engineered disulfide approach. We exchanged residues within the putative p-loop (Fig. 2B) to cysteine, anticipating a loss of channel function when disulfide bridges are formed due to sufficient proximity of cysteines within the tetrameric pore complex. In order to verify cysteine cross-linking, we tested for rescue of function by the reducing agent dithiothreitol (DTT). For these experiments, cells expressing TRPC3 or the respective mutant channel were preincubated with 5 mM DTT for 2 min and subsequently measured in the continuous presence of the compound. Fig. 2A depicts carbachol-evoked inward currents at −90 mV and outward currents at +70 mV recorded from wild type TRPC3 and indicated mutant channels in the absence or presence of DTT, respectively. Introduction of a cysteine at positions 630 or 631 completely abolished ion permeation yielding inward currents of -0.3 ± 0.26 pA/pF and -0.1 ± 0.05 pA/pF, respectively. Currents through these mutants were partially recovered by DTT, yielding inward currents of -2.8 ± 0.87 pA/pF for the E630C mutant and -1.9 ± 0.88 pA/pF for the V631C mutant channel. Likewise, the S629C mutant channel displayed strongly reduced inward currents (-1.07 ± 0.34 pA/pF), which were clearly restored by DTT (-5.9 ± 4.40 pA/pF). By contrast, substitution of

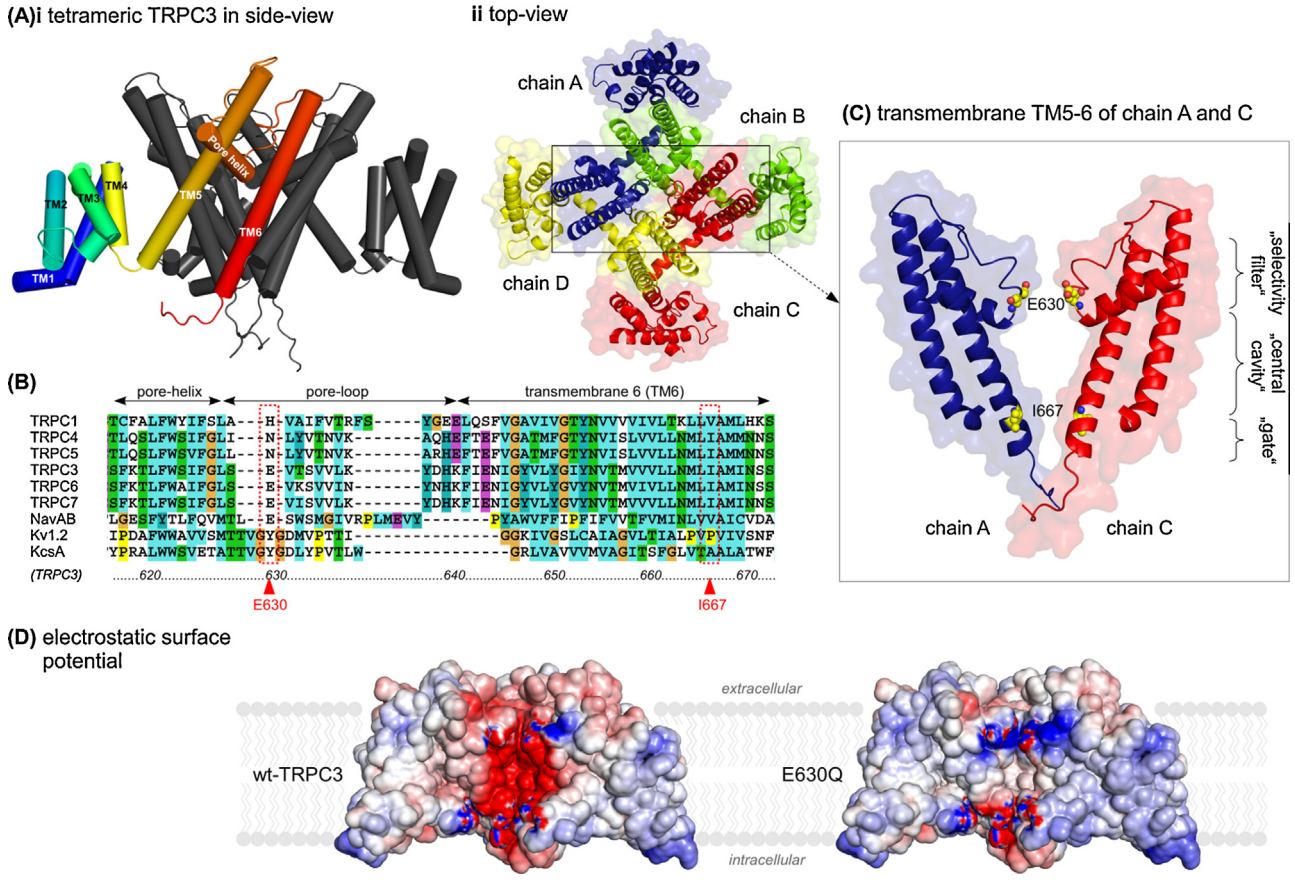

Fig. 1. Molecular modeling identifies residues with potential significance for ion selectivity and gating in TRPC3. Molecular model of human TRPC3, based on the structure of Na_VAB. (A) (i) Side view of structural domains in TRPC3. One subunit is colored according to the 6 transmembrane (TM) domains. The foremost TM1-TM4 module was removed for clarity. (ii) Top view of the four subunits (chain A–D) forming the complete TRPC3 tetramer. (B) Sequence alignment of the putative pore region of Na_VAB, KcsA, Kv1.2 and mammalian TRPC isoforms (TRPC1-TRPC7). E630 as the key element of the TRPC3 selectivity filter is conserved among closely related isoforms TRPC3/6/7. An isoleucine residue at the cytosolic end of TM6 (I667 in TRPC3) is largely conserved in TRPC channels and may contribute to the physical channel gate. (C) Excerpt showing the TM5-6 region (residue 570–680) of two opposing subunits A and C. Amino acid residues with potential significance for ion selectivity (E630) and gating (I667) are highlighted in yellow. (D) Solvent accessible electrostatic surface potential of wild type TRPC3 (wt-TRPC3) and E630Q mutant channel (E630Q) showing negative and positive potentials colored red and blue, respectively. TM1-4 of chain A and TM5-6 of chain B have been removed to uncover the permeation path.

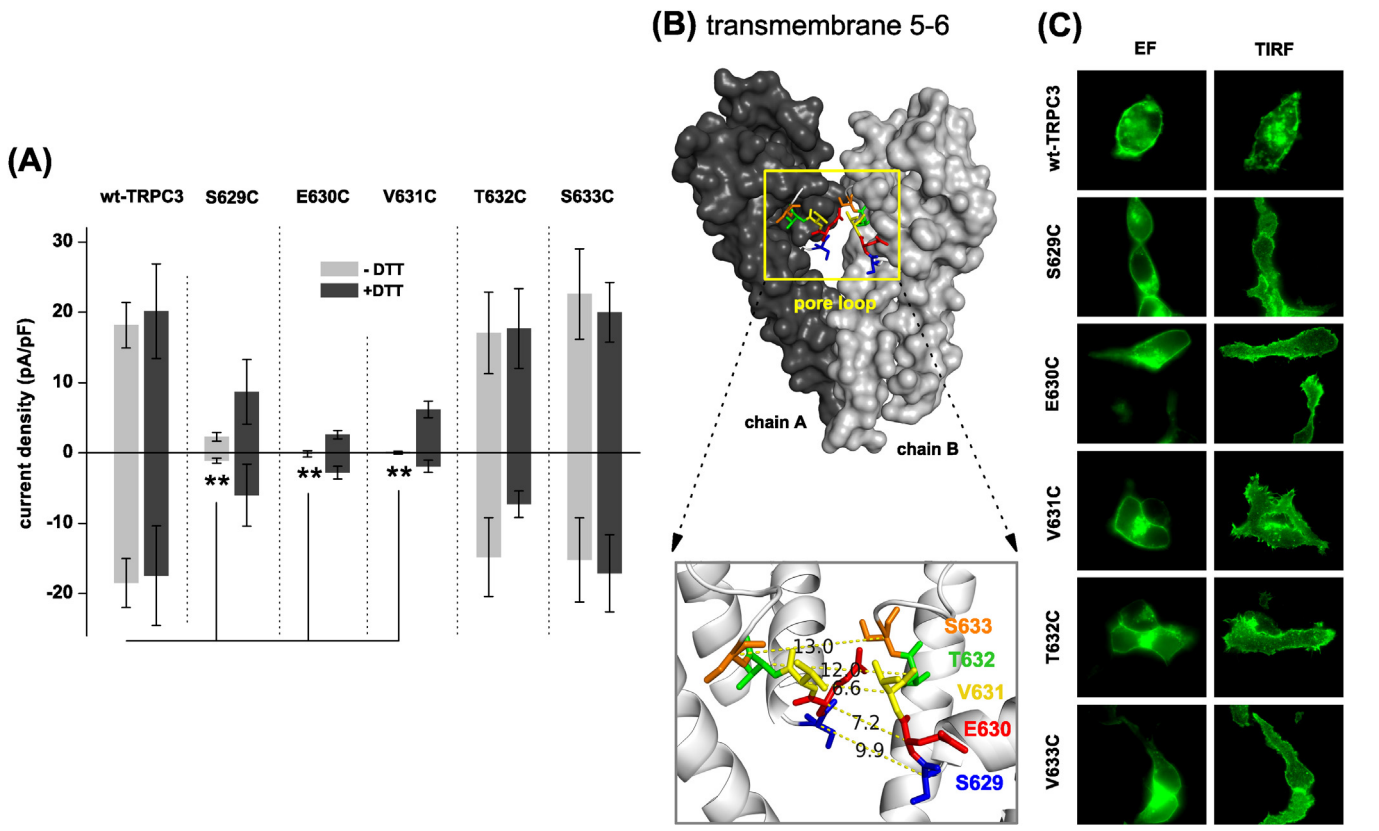

Fig. 2. An engineered disulfide approach identifies E630 and V631 as the narrowest region within the putative pore loop. (A) Histogram showing mean current densities at −90 mV and +70 mV recorded from carbachol (100 μM) – stimulated HEK293 cells expressing wild type TRPC3 or a mutant TRPC3 channel in which S629, E630, V631, T632 or S633 has been replaced by cysteine. Currents were recorded in the absence (−DTT) or after 3 min. preincubation and continuous presence of 5 mM dithiothreitol (+DTT). Data represent the mean ± S.E.M., $n > 7$. (B) Molecular model of the transmembrane 5–6 region of adjacent subunits A and B. Excerpt shows p-loop residues potentially forming the selectivity filter along with the corresponding inter-subunit distance (Å). (C) Representative epifluorescence and TIRF microscopy images of HEK293 cells expressing wild type or the indicated mutant TRPC3 channel.

either T632 or S633 by cysteine generated channels that were functionally indistinguishable from wild type TRPC3. Inward currents in the absence and presence of DTT, respectively, amounted to −14.8 ± 5.61 pA/pF and −7.3 ± 1.88 pA/pF for the T632C mutant and to −15.2 ± 5.99 pA/pF and −17.1 ± 5.5 pA/pF for the S633 C mutant as compared to −18.5 ± 3.47 pA/pF and −17.5 ± 7.07 pA/pF for the wild type channel. Notably, in the presence of DTT, currents through the V631C mutant showed enhanced outward rectification along with a significant shift in reversal potential (−18 ± 3 mV) compared to the wild type channel (9.1 ± 0.79 mV). This finding suggests altered selectivity as a consequence of introducing a cysteine close to the "selectivity filter glutamate" E630. A similar tendency of promoted rectification was observed for the T632C mutant. Nevertheless, reversal potentials of T632C in the presence of DTT were not significantly different from T632C in the absence of DTT or wild type TRPC3. Membrane presentation of tested channel proteins was confirmed by epifluorescence- and TIRF-microscopy (Fig. 2C).

Collectively, our findings suggest that the distance between cysteines introduced at positions 632 or 633 is large enough to prevent cross-linking whereas cysteines introduced at positions 629, 630 and 631 appear close enough to allow for disulfide-bond formation. Hence, we locate the narrowest region within the TRPC3 p-loop to positions 629–631.

3.2. E630 determines pore size and sensitivity of TRPC3 to ruthenium red

In order to assess whether neutralization of E630 affects ion selectivity by simply removing an electrostatic interaction site for divalents or due to larger rearrangements in pore architecture, we probed the pore dimensions of the wild type channel in comparison to the E630Q mutant. The limiting pore diameter was deduced from the permeabilities of organic monovalent cations of various sizes. Whole-cell recordings were started in physiological standard solution, TRPC3 currents were activated by carbachol and extracellular Na^+ was rapidly exchanged for different ammonium ions after obtaining the maximum current response. Both, wild type TRPC3 (Fig. 3Ai) and E630Q mutant channels (Fig. 3Aii) clearly allowed permeation of DMA^+. Interestingly, the switch to DMA^+ generated even a moderate current increase. Switch to $TriMA^+$ did not affect the typical slow current decay of TRPC3 wild type channel activity significantly but led to a rapid decline of E630Q currents. Fig. 3B shows a comparison of the current decay recorded from wild type and E630Q channels within 10 s after switch to $TriMA^+$ given as % of the maximum current at −90 mV. Currents declined by 30.6 ± 2.85% in wild type TRPC3 and by 72.7 ± 14.85% in the E630Q mutant, indicating substantially reduced permeation in the mutant. Exchange of Na^+ for $TetMA^+$ produced a sharp decline of current in both wild type and E630Q mutant, demonstrating that channels are fairly impermeable for this large ammonium ion. Thus, neutralizing the negative charge at position 630 within the putative p-loop slightly decreases the pore diameter of wild type TRPC3 from <5.8 Å to <5.2 Å in the mutant channel. This finding was corroborated by functional analysis of cysteine pore mutants (Fig. 3C). As outlined above, exchange of T632 to cysteine in wild type TRPC3 did not significantly reduce current flow, suggesting that proximity between cysteines is insufficient for disulfide bond formation. By contrast, introduction of a cysteine at position

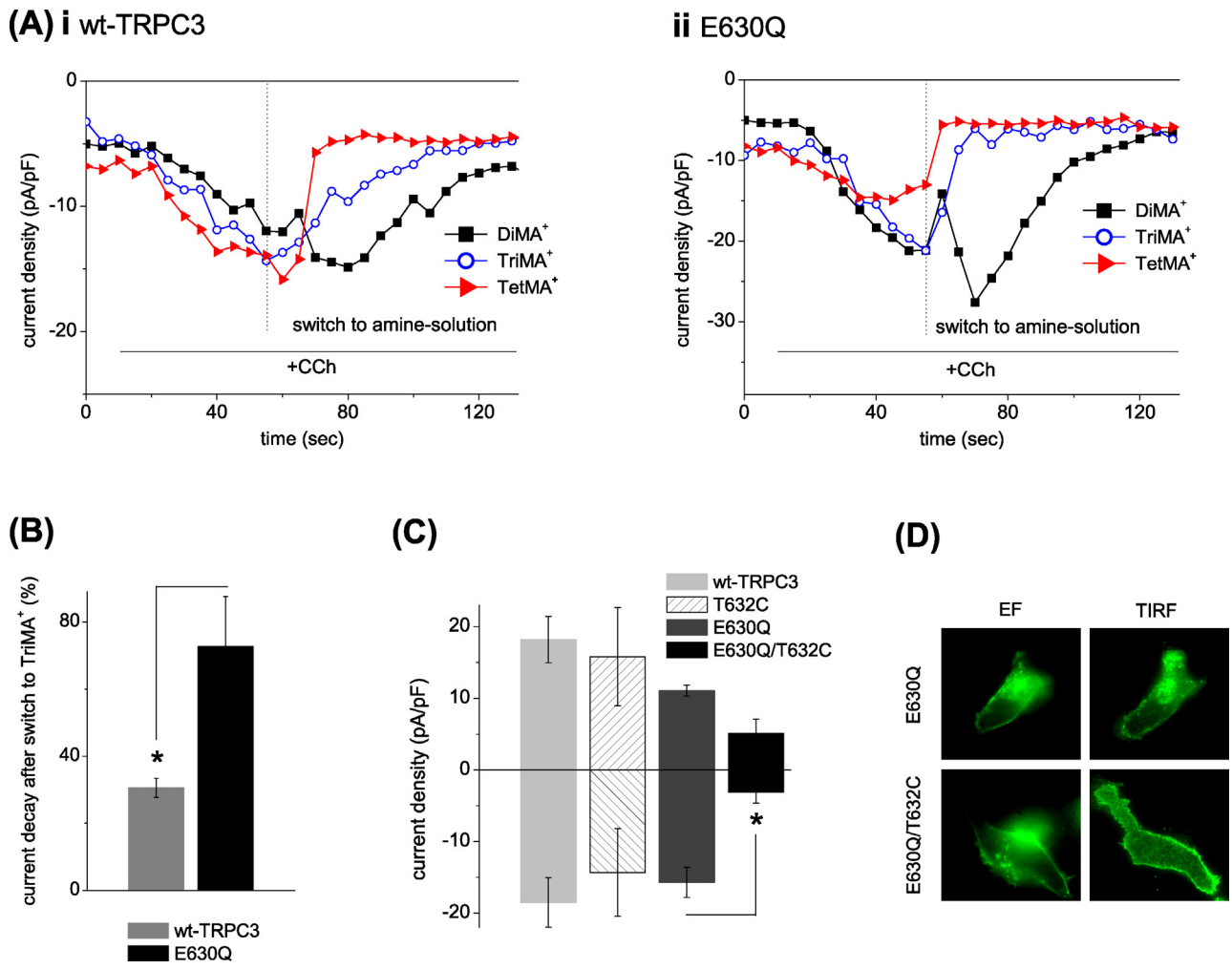

Fig. 3. Neutralization of glutamate E630 reduces the pore diameter of wild type TRPC3. (A) Representative time courses of current during acute amine administration. Inward currents at −90 mV through wild type TRPC3 (i) or E630Q mutant channel (ii) stimulated by 100 μM carachol are shown. Dashed lines indicate the switch from standard ECS to solutions in which sodium was equimolarly replaced by the respective amine. (B) Columns show the mean current decay 10 s after switch to amine solution in wild type TRPC3 and E630Q mutant channel. Data are expressed as % of the maximum response at −90 mV. Data represent the mean ± S.E.M., $n > 6$. (C) Histogram illustrating mean carbachol (100 μM)-stimulated current densities at +70 mV and −90 mV through either wild type TRPC3, T632 C mutant, E630 mutant or E630Q/T632 C double mutant channels. Data represent the mean ± S.E.M., $n > 6$. (D) Representative epifluorescence and TIRF microscopy images of HEK293 cells expressing E630Q or E630Q/T632C double mutant channel.

632 into E630Q-background dramatically reduced inward currents from −15.7 ± 2.11 pA/pF to −3.1 ± 1.53 pA/pF in the E630Q/T632 C mutant. Treatment of cells expressing the E630Q/T632C mutant with DTT resulted in moderate but statistically significant increase in current (5.5 ± 1.17 pA/pF, data not shown), which substantiates ormation of disulfide bonds in the double mutant. Proper membrane targeting of tested mutant TRPC3 channels was confirmed by epifluorescence- and TIRF-microscopy (Fig. 3D). The finding that a cysteine introduced at position 632 is able to form disulfide bonds only in the E630Q mutant background, indicates that neutralization of E630 reduces the pore diameter of TRPC3 to an extent that allows cysteine cross-linking.

As rearrangements in the pore architecture are expected to impact on sensitivity of channels to blockers, we investigated sensitivity of the E630Q mutant to ruthenium red (RR). RR is a hexavalent cation known as a classical voltage-dependent pore blocker of different TRP channel species [20–22]. Moreover, it has recently been shown that RR inhibits non-selective cation currents in dorsal root ganglion neurons that were ascribed to TRPC3 [23]. In our study, RR was permanently present throughout the entire experiment. Extracellular application of 3 μM RR (Fig. 4A) markedly suppressed TRPC3 inward currents without significant changes in outward currents as expected from a voltage-dependent pore block. As illustrated (insert), inward currents at −90 mV were reduced to −1.95 ± 0.49 pA/pF whereas the outward currents at +70 mV remained unchanged despite the presence of RR (17.9 ± 2.72 pA/pF). The reversal potential was shifted toward negative values (−19.3 ± 2.66 mV, data not shown). In clear contrast, the E630Q mutant channel was completely insensitive to extracellular application of RR. Inward currents (−14.1 ± 4.35 pA/pF) and outward currents (9.47 ± 2.54 pA/pF) were not significantly different from those measured in the absence of RR (inward: −15.7 ± 2.11 pA/pF; outward: 11.1 ± 0.77 pA/pF). Since it has recently been shown that TRPV1 is inhibited by both, extracellular and intracellular RR [24], we performed further experiments in which 3 μM RR was applied from the intracellular side via the patch pipette solution (Fig. 4B). Application of RR (even up to 10 μM, data not shown) from the intracellular side failed to affect current through either wild type TRPC3 or E630Q mutant channel. Thus, we demonstrate that neutralization of a negatively charged residue (E630) at the extracellular boundary of the putative selectivity filter abrogates sensitivity of TRPC3 channels to the pore blocker RR. Hence, E630 is likely to determine ion selectivity by providing an interaction site for permeating divalents and by

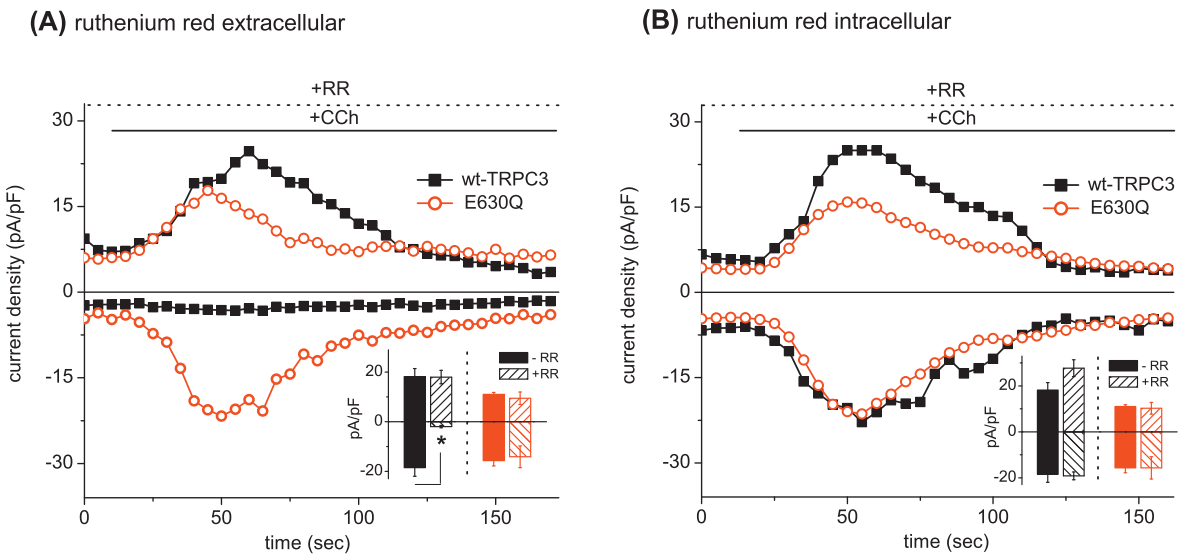

Fig. 4. E630Q mutation abolishes sensitivity of TRPC3 to voltage-dependent pore blocker ruthenium red. (A) Representative time courses of carbachol (100 μM) – evoked current at −90 mV and +70 mV through wild type TRPC3 or E630Q mutant channel expressed in HEK293 cells. Extracellular administration of 3 μM ruthenium red (RR) via the bath solution is shown on the left (i) and intracellular administration via the patch pipette is shown on the right (ii). Inserts present statistics of currents densities recorded from wild type TRPC3 (black) and E630Q mutant channel (red) in the absence (−RR) or in the presence of ruthenium red (+RR). Data are presented as the mean ± S.E.M., $n > 5$.

stabilizing the architecture of the selectivity filter. Moreover, this acidic residue is essential for sensitivity of TRPC3 to ruthenium red.

3.3. E630 is not essential for monovalent permeation through TRPC3

As evident from the multiple sequence alignment in Fig. 1B, E630 is aligned with the selectivity filter glutamate in Na_VAB [10] and the GYG-signature sequence of KcsA and Kv1.2 that constitutes a pivotal element of the selectivity filter in potassium channels [25]. Having identified E630 as required for divalent permeation, we asked whether this residue would as well govern the permeation of monovalent cations. Hence, we compared the permeability features of wild type and E630Q mutant channel in terms of the Eisenman permeability sequence for monovalent cations (Fig. 5). Since classical carbachol-evoked TRPC3 currents are transient in nature, whole-cell voltage-clamp experiments were performed in a solution containing a single monovalent cation and permeabilities were deduced from the obtained reversal potentials. Superfusion of 100 μM carbachol was used to stimulate Na^+-, Cs^+-, K^+-, and Rb^+-currents, whereas Li^+-currents were provoked by the synthetic DAG-analog SAG in order to circumvent inhibitory effects of Li^+ on G-protein signaling [26,27]. For wild type TRPC3, replacing extracellular sodium by other monovalent cations produced only moderate changes in reversal potential, suggesting that the TRPC3 selectivity filter poorly discriminates between diverse monovalent species. The obtained permeability sequence as deduced from reversal potentials after correction for liquid junction potential is shown in Fig. 5A: $Li^+(-5.1 \pm 2.33\,mV) < Na^+(0.3 \pm 0.8\,mV) < Cs^+(6.6 \pm 0.86\,mV) < K^+(6.9 \pm 1.02\,mV) < Rb^+(8.7 \pm 3.54\,mV)$, corresponding to Eisenman III permeability sequence, which is indicative of a weak field strength binding site for monovalent cations. Interestingly, the E630Q mutant as well displayed the Eisenman III permeation profile. As depicted in Fig. 5A, reversal potentials and consequent permeability series was: $Li^+(-10.8 \pm 3.05\,mV) < Na^+(-0.14 \pm 2.74\,mV) < Cs^+(12.6 \pm 0.87\,mV) < K^+(12.8 \pm 1.06\,mV) < Rb^+(13.2 \pm 2.07\,mV)$. Fig. 5B illustrates the corresponding I/V-relations of monovalent currents through (i) wild type channel and (ii) E630Q mutant. In clear contrast to divalent permeation, we find that E630 does not contribute to the electrostatic field that determines permeation of monovalent cations through TRPC3. Strikingly, neither the change in electrostatic basis for divalent permeation nor the associated structural rearrangements of the pore domain affected monovalent permeation. These findings suggest that monovalent and divalent permeation through the TRPC3 channel are governed by distinct structures and mechanisms.

3.4. I667 is part of the physical channel gate at the cytosolic end of the TM6 helix

To identify structural motifs involved in gating of TRPC3, we first aimed to identify the residue(s), which occlude the channel in the resting state, referred to as the physical channel gate. Our template channel for molecular modeling Na_VAB, has been recently shown to exhibit a gate at the cytosolic bundle-crossing of the pore-forming helices [10]. By analogy, our molecular model predicted the main gate of TRPC3 located at the C-terminal end of the pore-forming TM6 domains. In detail, the TM6 helices delimit the central cavity and narrow toward the cytosol to form the hydrophobic channel gate that includes isoleucine I667 (Fig. 1C). Assuming that the large side chain volume of this isoleucine residue contributes to the hydrophobic seal, we hypothesized that mutational exchange to the smaller alanine would hamper channel closure. Indeed we found that the I667A mutant displays gain in function, which was first indicated by a reduced cell survival of HEK293 cells expressing this mutant. Electrophysiological characterization of cells expressing the I667A mutant revealed large, constitutive inward currents (-18.3 ± 1.94 pA/pF) and outward currents (22.6 ± 3.66 pA/pF) immediately after whole-cell break-in (Fig. 6A and D). Currents through I667A channels were further increased by application of carbachol, producing additional inward currents at −90 mV and outward currents at +70 mV of -9.1 ± 2.19 pA/pF and 18.2 ± 2.82 pA/pF, respectively (Fig. 6A and D). These results indicate that the I667A mutation severely destabilizes the occluding gate, resulting in significantly increased constitutive channel activity without generating a maximum TRPC3 conductance. Consistent with these findings, replacing I667 by charged glutamate produced a comparable enhancement of

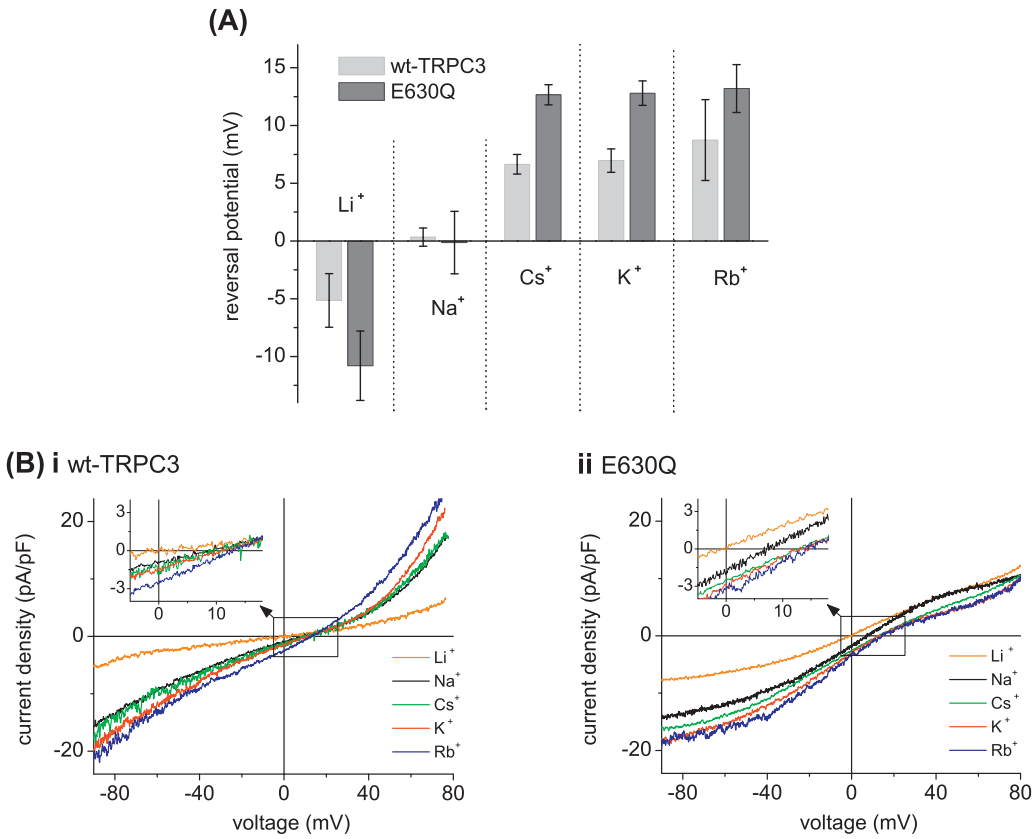

Fig. 5. Neutralization of E630 does not change the Eisenman permeation profile of monovalent cations. (A) Histogram showing mean reversal potentials of currents through wild type TRPC3 (wt-TRPC3) or E630Q mutant channels (E630Q) in a solution containing 140 mM of indicated monovalent cations. The permeation sequence $Li^+ < Na^+ < Cs^+ < K^+ < Rb^+$ determined for the wild type as well as for the E630Q mutant channel corresponds to the Eisenman III sequence. Reversal potentials are corrected for liquid junction potential. Data represent the mean ± S.E.M., $n > 10$. (B) Representative I/V-relations of carbachol (100 μM)-induced currents through wild type TRPC3 (i) or E630Q mutant channels (ii). Currents were recorded in the presence of 140 mM of the respective monovalent cation and reveal Eisenman III permeability sequence. Note that original traces are not corrected for liquid junction potential.

basal channel activity to a level of about 50% (data not shown). Interestingly, carbachol-evoked I667A currents did not display the transient nature of a classical TRPC3-response but remained stable for a few minutes (Fig. 6A), indicating that the gate mutant is unable to enter a certain de- or inactivated closed state after channel activation. To substantiate that the recorded currents indeed originate from TRPC3 activity, we tested for sensitivity to the pore blocker ruthenium red (RR). Importantly, extracellular administration of 3 μM RR clearly inhibited basal as well as carbachol-evoked current through the I667A mutant (Fig. 6A). It is of note that the I/V-relations of currents through wild type TRPC3 and I667A mutant (Fig. 6B) at time points indicated in (A) reveal a more linear profile in case of the mutant channel. In addition, we noticed a slight leftward shift in reversal potential for the I667A mutant (4.8 ± 2.76 mV) compared to the wild type (9.1 ± 0.79 mV) (Fig. 6C), pointing toward alterations in selectivity behavior. Structural rearrangements in the outer pore domain including the selectivity filter were further indicated by a slight but significant change in block by RR, which clearly suppressed outward currents in I667A but not in wild type channels (Fig. 6A). Consequently, we compared the Ca^{2+}-selectivity of wild type TRPC3 to the I667A mutant. As depicted in Fig. 6C, whole-cell currents recorded in a solution containing 10 mM Ca^{2+} as the sole charge carrier, yielded a dramatic leftward shifted reversal potential for the I667A mutant (−41 ± 1.64 mV) compared to the wild type (1.8 ± 1.39 mV), indicative of a profound reduction in Ca^{2+}-selectivity. The hypothesis that modification in the function of the occluding gate impacts on the structure of the selectivity filter, was further confirmed by applying the engineered disulfide approach. Introduction of a cysteine at position 629 within the selectivity filter led to robust disulfide bond formation in wild type TRPC3 whereas serine-to-cysteine mutation at the same position into I667A background did not disrupt functionality. As shown in Fig. 6D, negligible carbachol-induced inward currents at −90 mV (−1.07 ± 0.34 pA/pF) were recorded for the S629C mutant, whereas the I667A/S629C double mutant generated inward currents (−15.9 ± 6.11 pA/pF) comparable to those of the I667A mutant. Hence, the I667A mutation appears to increases the distance between residues at position 629. This finding strongly indicates alterations in the architecture of the selectivity filter along with the I667A mutation. Proper membrane targeting of tested TRPC3 mutants was confirmed by epifluorescence- and TIRF-microscopy (Fig. 6E).

In aggregate, our results provide evidence for allosteric coupling between the TRPC3 gate and selectivity filter.

4. Discussion

4.1. A structural model of the TRPC3 pore domain based on homology to Na_VAB

We present here a molecular model of the TRPC3 pore complex that uses the voltage-gated sodium channel Na_VAB as a template structure. Applying a homology-guided mutagenesis approach, we explored fundamental structure–function relations within the predicted pore region. Initially, the generated homology model was scrutinized by two mutational approaches, (i) probing accessibility and distance of p-loop residues using an engineered disulfide approach and (ii), determining the pore dimensions of the channel.

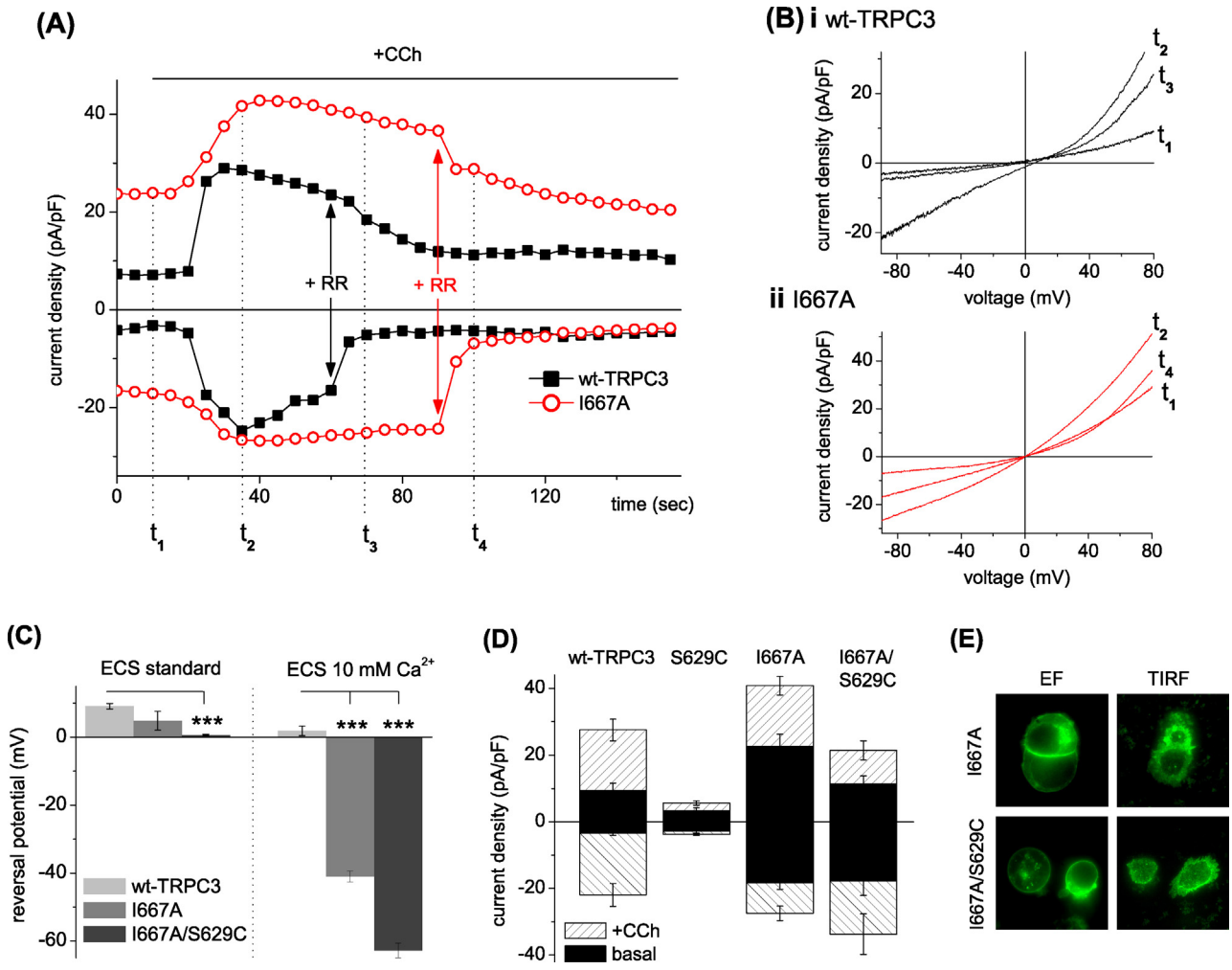

Fig. 6. I667 is part of the physical TRPC3 gate. (A) Representative time courses of currents at −90 mV and +70 mV recorded from HEK293 cells expressing wild type TRPC3 or I667A mutant channel. After cell stimulation with 100 μM carbachol (+CCh), 3 μM of the pore blocker ruthenium red (+RR) was administered as indicated. (B) I/V-relations of currents through wild type TRPC3 (i) and I667A mutant channels (ii) at time points indicated in (A). Note that traces are not corrected for liquid junction potential. (C) Histogram showing mean reversal potentials of currents through wild type TRPC3, I667A and I667A/S629C mutant channels in standard exracellular solution (ECS standard) and in a solution containing 10 mM Ca^{2+} as the sole charge carrier (ECS 10 mM Ca^{2+}). Data represent the mean ± S.E.M., $n > 6$. (D) Mean current densities at −90 mV and +70 mV of basal and carbachol-stimulated (+CCh) HEK293 cells expressing wild type TRPC3, S629 C, I667A or I667A/S629C double mutant channels. Data are presented as mean ± S.E.M., $n > 6$. (E) Representative epifluorescence- and TIRF-microscopy images of HEK293 cells expressing I667A or I667A/S629C double mutant channels.

Electrophysiological characterization of p-loop mutants revealed disulfide bond formation upon introduction of cysteine at positions central within the putative selectivity filter (629–631) whereas no cross-linking was observed at positions located at the putative pore entrance (632 and 633). This is in full accordance with the prediction of the molecular model and demonstrates that the narrowest region within the p-loop is formed by residues E630 and V631. As shown in Fig. 2B, the distance of Cα-atoms between these residues on neighboring subunits was predicted to be 7.2 Å and 6.6 Å, respectively. Since disulfide bond formation in proteins typically occurs at a distance between Cα-atoms of <7 Å [28], the proposed distance between residues at position 629 (9.9 Å) is quite large for cysteine cross-linking. Nonetheless, normal protein dynamics and conformational flexibility typically display an amplitude of up to 3 Å and thereby likely provide enough flexibility to enable disulfide bond formation at position 629. By contrast, residues T632 and S633 are predicted to localize at the outer pore entrance with a larger inter-subunit distance of 12 Å and 13 Å. Since cysteines introduced at three adjacent positions (629–631) within the p-loop are capable of cross-linking, we propose a non-helical selectivity filter defined by amino acid side chains that project toward the permeation path to govern selectivity mainly via the side chain of E630 as we have recently shown [7]. It is of note that some cysteine mutations adjacent to the critical glutamate residue (630) modified channel properties in addition to subunit crosslinking. DTT did not recover exact wild type current properties for positions 631 and 632 as evident from promoted rectification and altered reversal of currents for the V631 C mutant. These alterations are likely due to slight changes in structure of the selectivity filter by amino acid exchange within this critical part of the pore. The concept of a selectivity filter formed by the loop connecting the innermost transmembrane domains using negatively charged residues as key determinants of selectivity, has been proposed for several members of the TRP channel family including the *Drosophila* TRP [8], TRPM channels [29,30], TRPVs [31,32] and TRPAs [33]. Noteworthy, all of these studies used homology models based on the structure of the evolutionary distant potassium channels, which are known to exhibit a selectivity filter formed by carbonyls functions of the protein main chain instead of amino acid side chains. By contrast, the closer related voltage-gated sodium channel Na_VAB combines the features of a re-entrant pore loop and a selectivity filter determined by amino acid side chains [10,34]. Thus, we consider Na_VAB preferable to potassium channels in terms of modeling the pore of TRP channels.

Estimation of pore size from permeability for differently sized alkyl-ammonium ions corroborated a limiting pore diameter of <5.8 Å for TRPC3 homomeric complexes. Our findings are in line with studies addressing the pore dimensions of other members of the TRP superfamily such as the Ca^{2+}-selective TRPV6 (5.4 Å) [17] and TRPV5 (7.5 Å at pH = 7.4) [35]. Significantly larger pore dimensions were reported for classical non-selective channels of the TRP family such as TRPM6 (at least 11.5 Å) [36], TRPA1 (non-stimulated ~11 Å) [37], TRPP2 (at least 11 Å) [38] and TRPV1 (>6.8 Å) [39]. The finding that the pore size of the non-selective TRPC3 channel resembles those of selective representatives of the TRP family, indicates that its Ca^{2+}-permeation may be governed by electrostatic features rather than by spatial features of the permeation path. It is well established that Ca^{2+}-selectivity is achieved with a wide range of pore diameters. Starting with the tiny pore of ORAI1 (3.6 Å) [40] to the larger pores of T-type (5.1 Å) and L-type (6.2 Å) calcium channel [41] or TRPV6 (5.4 Å) and TRPV5 (7.5 Å) and finally reaching the huge pores of the Mg^{2+}/Ca^{2+}-selective TRPM6 (at least 11.5 Å). However, we find that the experimentally estimated pore diameter of TRPC3 (<5.8 Å) is close to that predicted from the molecular model (5–6 Å). Since potassium channels, which have repeatedly been used for molecular modeling of TRP channels, display much smaller pore diameters of close to 3 Å, we again regard Na_VAB preferable for modeling.

Since our functional characterization of TRPC3 mutants was perfectly consistent with the molecular architecture predicted by homology modeling we suggest suitability of the template structure Na_VAB.

4.2. The TRPC3 selectivity filter

Identification of E630 within the putative p-loop as the key element of divalent permeation led to the question whether this residue would as well determine monovalent permeation. Surprisingly, wild type as well as E630Q mutant channels were characterized by the Eisenman III permeability sequence. In clear contrast to permeation of divalent cations, the negative charge of E630 apparently lacks impact on conduction of monovalent cations. These findings are in line with studies addressing this issue in other members of the TRP family. Recently, murine TRPC6 was reported to exhibit the Eisenman III permeation profile given by relative permeabilities as follows: $P_{Li+}(0.77) < P_{Na+}(1) = P_{Cs+}(1) < P_{K+}(1.06) < P_{Rb+}(1.12)$ [42] and comparable results were obtained for human TRPC6 [43]. This similarity in pore properties of TRPC3 and TRPC6 is in conflict with an earlier study classifying TRPC3 expressed in bovine pulmonary artery endothelial cells with a strong-field strength binding site for monovalent cations given by the permeability order: $P_{Na+} > P_{Cs+} = P_{K+}$ [44]. Expression levels of endogenous TRPC proteins is expected to differ between endothelial and HEK293 cells. Thus, a certain amount of heteromerization is anticipated for native channels in endothelial cells and may explain the observed discrepancy in selectivity behavior. Weak field strength binding sites for monovalent cations have also been reported for TRPM7 [30] and the non-selective TRPV subtypes TRPV1 [45], TRPV2 and TRPV4 [31]. The latter was reported to display the Eisenman IV permeation order for monovalent cations. Consistent with our findings in TRPC3, separate mutational neutralization of two aspartate residues identified as key elements of the TRPV4 selectivity filter, did not alter the channel's Eisenman sequence. Likewise, mutational neutralization of the "selectivity-filter-aspartate" in TRPV5 did not change the monovalent permeability order [32]. In summary, our findings indicate the existence of two fairly independent permeation mechanisms in TRPC3. While conductance of divalent cations is dependent on E630, monovalent permeation may be governed by other charged moieties along the permeation path such as helix-dipoles.

Our molecular model predicted profound changes in electrostatics of the permeation path upon neutralization of E630 (Fig. 1D), which was found to impact on pore architecture and sensitivity to pore blockers. We identified a reduction of the pore size in the E630Q mutant by 0.4 Å. Thus, E630 appears to affect TRPC3 selectivity behavior by stabilizing the global structure of the p-loop region. Furthermore, we found that removal of charge in position 630 eliminates sensitivity to the voltage-dependent pore blocker ruthenium red (RR). This poly-cationic dye acts as a pan inhibitor on a wide range of cation channels including ryanodine receptors, mitochondrial calcium transporters, CatSper1, TASK and moreover all members of the TRPV family as well as TRPM6 and TRPA1 [20–22,46,47]. Apart from a recent report on RR inhibiting a non-selective cation current in rat dorsal root ganglion neurons that was accounted to TRPC3 [23], little is known about the effect of RR on TRPC channels. However, we observed a potent voltage-dependent blocking action of RR on TRPC3, which was fully eliminated by the E630Q mutation. Thus, this negatively charged residue is essentially involved in interaction of RR with the TRPC3 channel pore. This is consistent with respective structure function relations in TRPV1 and TRPV4, where a single aspartate within the pore loop was identified as molecular determinant of RR sensitivity [21,31]. Similarly, block of TRPM6 by RR appeared to depend on Glu1029 and adjacent Ile1030 [36]. In line with this, our results imply that RR blocks the pore of TRPC3 from the extracellular side by reversible, electrostatic interaction with E630.

Altogether, we suggest E630 as a charged residue within the pore loop of TRPC3 that critically determines divalent permeation, pore architecture and sensitivity to a common pore blocker.

4.3. Potential linkage between gate and selectivity filter

In a number of ion channels, the physical gate was localized to the cytosolic termini of the pore-forming helices. Specifically, the innermost helices narrow toward the cytosolic face and finally cross each other to occlude the pore at the bottom of the channel. This so-called "helix-bundle-crossing" gate classically contains amino acids with bulky, neutral side chains that form a hydrophobic seal. Such a main activation gate was found in mechanosensitive channels, ligand-gated channels, potassium channels [48–51] and also sodium channels such as Na_VAB [10], which was used here as template for molecular modeling. In consequence, our hypothetical model predicted the TRPC3 gate to be located at the cytosolic end of the pore-forming TM6 domain (Fig. 1C). We identified I667 within this region as a residue essential for proper channel closure. Introduction of alanine or glutamate at this position severely destabilized the hydrophobic seal and rendered the channel constitutively active, implying that the channels gate lost stability to reside in a closed conformation. Thus, we suggest an isoleucine residue (I667) at the C-terminal end of the pore-forming TM6 helix to be part of the main activation gate of TRPC3. Hitherto, no crystal structure is available for any TRP channel, but substantial first insights into 3D structure of TRPC3 at 15 Å resolution were obtained with cryo-electron microscopy [52]. This study suggested the TRPC3 channel gate to be located at the level of the cytosolic face of the inner leaflet of the membrane bilayer, which is in full accordance with our findings. Expression of the I667A mutant in HEK293 clearly decreased overall cell viability, reminiscent of other gain-in-function mutations such as the murine TRPC3-moonwalker mutation [7]. Surprisingly, we found that the I667A mutant generated an unusual sensitivity of outward currents to the pore blocker RR. In addition, the Ca^{2+}-permeability of the mutant was dramatically reduced, corresponding to a decline in the Ca^{2+}/Cs^{+}-permeability ratio from 3.7 to approximately 0.1 in the mutant. These findings led us to hypothesize that reduced gating stability may impact on the outer pore structure including the

selectivity filter. This was confirmed by the observation that the gate-destabilizing I667A mutation prevented cysteine crosslinking in the selectivity filter for cysteine introduction in position 629. The observation that a single point mutation within the occluding gate is associated with alterations in ion permeation, sensitivity to external block by RR and disulfide bond formation in the selectivity filter suggests tight coupling between selectivity and gating in TRPC3. Similar functional linkage between gate and pore helix in p-loop channels has been suggested previously for other channels. Motion of the pore helix was reported to regulate gating or to function as a secondary gate in p-loop channels such as cyclic nucleotide-gated channels [53], voltage-gated calcium channels [54] and voltage-gated sodium channels [55]. Recently, a similar concept was put forward for TRPV channels. Inhibitory gating of TRPV5 by intracellular acidification was shown to be associated with a conformational rearrangement of the pore helix described as a clockwise rotation about its axis [35]. In consequence, gating of TRPV channels was suggested to involve two coordinated components of motion: a hinged movement of the inner helices to open the main activation gate at the cytosolic helix-bundle crossing combined with a rotation of the pore helices within the p-loop as the secondary gate [56]. On the assumption that similar holds true for the related TRPC channels, we propose that the TRPC3 main activation gate is linked in an allosteric fashion to the pore loop as a secondary gate. This may explain our observation, that mutational destabilization of the main gate is associated with a change in selectivity behavior.

Collectively, our results demonstrate suitability of the Na_VAB structure for molecular modeling of the TRPC family. Based on this modeling approach, we identified key determinants of TRPC3 permeation and gating and revealed a potential structural and functional link between occluding gate and selectivity filter in the TRPC3 channel.

Acknowledgements

This work was supported by FWF grants P22565-B19 to CR and P21925-B19 to KG and DK+ Metabolic and Cardiovascular Disease grant W2126-B18.

References

[1] C. Rosker, A. Graziani, M. Lukas, P. Eder, M.X. Zhu, C. Romanin, K. Groschner, Ca(2+) signaling by TRPC3 involves Na(+) entry and local coupling to the Na(+)/Ca(2+) exchanger, The Journal of Biological Chemistry 279 (2004) 13696–13704.
[2] D. Poburko, C.H. Liao, V.S. Lemos, E. Lin, Y. Maruyama, W.C. Cole, C. van Breemen, Transient receptor potential channel 6-mediated, localized cytosolic [Na^+] transients drive Na^+/Ca^{2+} exchanger-mediated Ca^{2+} entry in purinergically stimulated aorta smooth muscle cells, Circulation Research 101 (2007) 1030–1038.
[3] P. Eder, M. Poteser, C. Romanin, K. Groschner, Na(+) entry and modulation of Na(+)/Ca(2+) exchange as a key mechanism of TRPC signaling, Pflügers Archiv 451 (2005) 99–104.
[4] K. Groschner, C. Rosker, TRPC3: a versatile transducer molecule that serves integration and diversification of cellular signals, Naunyn-Schmiedeberg's Archives of Pharmacology 371 (2005) 251–256.
[5] T. Hofmann, M. Schaefer, G. Schultz, T. Gudermann, Subunit composition of mammalian transient receptor potential channels in living cells, Proceedings of the National Academy of Sciences of the United States of America 99 (2002) 7461–7466.
[6] X. Liu, B.B. Singh, I.S. Ambudkar, TRPC1 is required for functional store-operated Ca^{2+} channels: role of acidic amino acid residues in the S5-S6 region, The Journal of Biological Chemistry 278 (2003) 11337–11343.
[7] M. Poteser, H. Schleifer, M. Lichtenegger, M. Schernthaner, T. Stockner, C.O. Kappe, T.N. Glasnov, C. Romanin, K. Groschner, PKC-dependent coupling of calcium permeation through transient receptor potential canonical 3 (TRPC3) to calcineurin signaling in HL-1 myocytes, Proceedings of the National Academy of Sciences of the United States of America 108 (2011) 10556–10561.
[8] C.H. Liu, T. Wang, M. Postma, A.G. Obukhov, C. Montell, R.C. Hardie, In vivo identification and manipulation of the Ca^{2+} selectivity filter in the *Drosophila* transient receptor potential channel, The Journal of Neuroscience 27 (2007) 604–615.
[9] B.A. McNally, A. Somasundaram, M. Yamashita, M. Prakriya, Gated regulation of CRAC channel ion selectivity by STIM1, Nature 482 (2012) 241–245.
[10] J. Payandeh, T. Scheuer, N. Zheng, W.A. Catterall, The crystal structure of a voltage-gated sodium channel, Nature 475 (2011) 353–358.
[11] T.J. Jegla, C.M. Zmasek, S. Batalov, S.K. Nayak, Evolution of the human ion channel set, Combinatorial Chemistry & High Throughput Screening 12 (2009) 2–23.
[12] R.C. Edgar, MUSCLE: multiple sequence alignment with high accuracy and high throughput, Nucleic Acids Research 32 (2004) 1792–1797.
[13] R. Aurora, G.D. Rose, Helix capping, Protein Science 7 (1998) 21–38.
[14] A. Sali, T.L. Blundell, Comparative protein modelling by satisfaction of spatial restraints, Journal of Molecular Biology 234 (1993) 779–815.
[15] M.Y. Shen, A. Sali, Statistical potential for assessment and prediction of protein structures, Protein Science 15 (2006) 2507–2524.
[16] R.A. Laskowski, J.A. Rullmann, M.W. MacArthur, R. Kaptein, J.M. Thornton, AQUA and PROCHECK-NMR: programs for checking the quality of protein structures solved by NMR, Journal of Biomolecular NMR 8 (1996) 477–486.
[17] T. Voets, A. Janssens, G. Droogmans, B. Nilius, Outer pore architecture of a Ca^{2+}-selective TRP channel, The Journal of Biological Chemistry 279 (2004) 15223–15230.
[18] C. Notredame, D.G. Higgins, J. Heringa, T-Coffee: a novel method for fast and accurate multiple sequence alignment, Journal of Molecular Biology 302 (2000) 205–217.
[19] M. Kamouchi, S. Philipp, V. Flockerzi, U. Wissenbach, A. Mamin, L. Raeymaekers, J. Eggermont, G. Droogmans, B. Nilius, Properties of heterologously expressed hTRP3 channels in bovine pulmonary artery endothelial cells, Journal of Physiology (London) 518 (1999) 345–358.
[20] D.E. Clapham, SnapShot: mammalian TRP channels, Cell 129 (2007), 220–220.
[21] C. Garcia-Martinez, C. Morenilla-Palao, R. Planells-Cases, J.M. Merino, A. Ferrer-Montiel, Identification of an aspartic residue in the p-loop of the vanilloid receptor that modulates pore properties, The Journal of Biological Chemistry 275 (2000) 32552–32558.
[22] H. Watanabe, J.B. Davis, D. Smart, J.C. Jerman, G.D. Smith, P. Hayes, J. Vriens, W. Cairns, U. Wissenbach, J. Prenen, V. Flockerzi, G. Droogmans, C.D. Benham, B. Nilius, Activation of TRPV4 channels (hVRL-2/mTRP12) by phorbol derivatives, The Journal of Biological Chemistry 277 (2002) 13569–13577.
[23] L. Qu, Y. Li, X. Pan, P. Zhang, R.H. LaMotte, C. Ma, Transient receptor potential canonical 3 (TRPC3) is required for IgG immune complex-induced excitation of the rat dorsal root ganglion neurons, The Journal of Neuroscience 32 (2012) 9554–9562.
[24] M. Luebbert, D. Radtke, R. Wodarski, N. Damann, H. Hatt, C.H. Wetzel, Direct activation of transient receptor potential V1 by nickel ions, Pflügers Archiv 459 (2010) 737–750.
[25] L. Heginbotham, Z. Lu, T. Abramson, R. MacKinnon, Mutations in the K^+ channel signature sequence, Biophysical Journal 66 (1994) 1061–1067.
[26] S. Avissar, G. Schreiber, A. Danon, R.H. Belmaker, Lithium inhibits adrenergic and cholinergic increases in GTP binding in rat cortex, Nature 331 (1988) 440–442.
[27] H.Y. Wang, E. Friedman, Effects of lithium on receptor-mediated activation of G proteins in rat brain cortical membranes, Neuropharmacology 38 (1999) 403–414.
[28] B.A. Katz, A. Kossiakoff, The crystallographically determined structures of atypical strained disulfides engineered into subtilisin, The Journal of Biological Chemistry 261 (1986) 15480–15485.
[29] B. Nilius, J. Prenen, A. Janssens, G. Owsianik, C. Wang, M.X. Zhu, T. Voets, The selectivity filter of the cation channel TRPM4, The Journal of Biological Chemistry 280 (2005) 22899–22906.
[30] M. Li, J. Du, J. Jiang, W. Ratzan, L.T. Su, L.W. Runnels, L. Yue, Molecular determinants of Mg^{2+} and Ca^{2+} permeability and pH sensitivity in TRPM6 and TRPM7, The Journal of Biological Chemistry 282 (2007) 25817–25830.
[31] T. Voets, J. Prenen, J. Vriens, H. Watanabe, A. Janssens, U. Wissenbach, M. Bodding, G. Droogmans, B. Nilius, Molecular determinants of permeation through the cation channel TRPV4, The Journal of Biological Chemistry 277 (2002) 33704–33710.
[32] B. Nilius, R. Vennekens, J. Prenen, J.G. Hoenderop, G. Droogmans, R.J. Bindels, The single pore residue Asp542 determines Ca^{2+} permeation and Mg^{2+} block of the epithelial Ca^{2+} channel, The Journal of Biological Chemistry 276 (2001) 1020–1025.
[33] B. Nilius, J. Prenen, G. Owsianik, Irritating channels: the case of TRPA1, Journal of Physiology 589 (2011) 1543–1549.
[34] F.H. Yu, W.A. Catterall, Overview of the voltage-gated sodium channel family, Genome Biology 4 (2003) 207.
[35] B.I. Yeh, Y.K. Kim, W. Jabbar, C.L. Huang, Conformational changes of pore helix coupled to gating of TRPV5 by protons, The EMBO Journal 24 (2005) 3224–3234.
[36] C.N. Topala, W.T. Groenestege, S. Thebault, D. van den Berg, B. Nilius, J.G. Hoenderop, R.J. Bindels, Molecular determinants of permeation through the cation channel TRPM6, Cell Calcium 41 (2007) 513–523.
[37] Y. Karashima, J. Prenen, K. Talavera, A. Janssens, T. Voets, B. Nilius, Agonist-induced changes in Ca(2+) permeation through the nociceptor cation channel TRPA1, Biophysical Journal 98 (2010) 773–783.
[38] G.I. Anyatonwu, B.E. Ehrlich, Organic cation permeation through the channel formed by polycystin-2, The Journal of Biological Chemistry 280 (2005) 29488–29493.
[39] N. Hellwig, T.D. Plant, W. Janson, M. Schafer, G. Schultz, M. Schaefer, TRPV1 acts as proton channel to induce acidification in nociceptive neurons, The Journal of Biological Chemistry 279 (2004) 34553–34561.

[40] M. Yamashita, L. Navarro-Borelly, B.A. McNally, M. Prakriya, Orai1 mutations alter ion permeation and Ca^{2+}-dependent fast inactivation of CRAC channels: evidence for coupling of permeation and gating, The Journal of General Physiology 130 (2007) 525–540.
[41] M. Cataldi, E. Perez-Reyes, R.W. Tsien, Differences in apparent pore sizes of low and high voltage-activated Ca^{2+} channels, The Journal of Biological Chemistry 277 (2002) 45969–45976.
[42] M. Estacion, W.G. Sinkins, S.W. Jones, M.A. Applegate, W.P. Schilling, Human TRPC6 expressed in HEK 293 cells forms non-selective cation channels with limited Ca^{2+} permeability, The Journal of Physiology 572 (2006) 359–377.
[43] T. Hofmann, A.G. Obukhov, M. Schaefer, C. Harteneck, T. Gudermann, G. Schultz, Direct activation of human TRPC6 and TRPC3 channels by diacylglycerol, Nature 397 (1999) 259–263.
[44] M. Kamouchi, S. Philipp, V. Flockerzi, U. Wissenbach, A. Mamin, L. Raeymaekers, J. Eggermont, G. Droogmans, B. Nilius, Properties of heterologously expressed hTRP3 channels in bovine pulmonary artery endothelial cells, The Journal of Physiology 518 (Pt 2) (1999) 345–358.
[45] M.J. Caterina, T.A. Rosen, M. Tominaga, A.J. Brake, D. Julius, A capsaicin-receptor homologue with a high threshold for noxious heat, Nature 398 (1999) 436–441.
[46] F. Vincent, M.A. Duncton, TRPV4 agonists and antagonists, Current Topics in Medicinal Chemistry 11 (2011) 2216–2226.
[47] T. Voets, B. Nilius, S. Hoefs, A.W. van der Kemp, G. Droogmans, R.J. Bindels, J.G. Hoenderop, TRPM6 forms the Mg^{2+} influx channel involved in intestinal and renal Mg^{2+} absorption, The Journal of Biological Chemistry 279 (2004) 19–25.
[48] D.A. Doyle, Structural changes during ion channel gating, Trends in Neurosciences 27 (2004) 298–302.
[49] R. MacKinnon, Potassium channels, FEBS Letters 555 (2003) 62–65.
[50] C. Kung, P. Blount, Channels in microbes: so many holes to fill, Molecular Microbiology 53 (2004) 373–380.
[51] D.A. Doyle, J. Morais Cabral, R.A. Pfuetzner, A. Kuo, J.M. Gulbis, S.L. Cohen, B.T. Chait, R. MacKinnon, The structure of the potassium channel: molecular basis of K^+ conduction and selectivity, Science 280 (1998) 69–77.
[52] K. Mio, T. Ogura, S. Kiyonaka, Y. Hiroaki, Y. Tanimura, Y. Fujiyoshi, Y. Mori, C. Sato, The TRPC3 channel has a large internal chamber surrounded by signal sensing antennas, Journal of Molecular Biology 367 (2007) 373–383.
[53] J. Liu, S.A. Siegelbaum, Change of pore helix conformational state upon opening of cyclic nucleotide-gated channels, Neuron 28 (2000) 899–909.
[54] X.G. Zhen, C. Xie, A. Fitzmaurice, C.E. Schoonover, E.T. Orenstein, J. Yang, Functional architecture of the inner pore of a voltage-gated Ca^{2+} channel, The Journal of General Physiology 126 (2005) 193–204.
[55] D.L. Capes, M. Arcisio-Miranda, B.W. Jarecki, R.J. French, B. Chanda, Gating transitions in the selectivity filter region of a sodium channel are coupled to the domain IV voltage sensor, Proceedings of the National Academy of Sciences of the United States of America 109 (2012) 2648–2653.
[56] S. Heller, R.G. O'Neil, Molecular mechanisms of TRPV4 gating, in: W.B. Liedtke, S. Heller (Eds.), TRP Ion Channel Function in Sensory Transduction and Cellular Signaling Cascades, CRC Press, Boca Raton, FL, 2007 (chapter 8).